Structure, Vol. 13, 817–824, May, 2005, ©2005 Elsevier Ltd All rights reserved. DOI 10.1016/j.str.2005.03.008

2-Oxoquinoline 8-Monooxygenase Oxygenase Component: Active Site Modulation by Rieske-[2Fe-2S] Center Oxidation/Reduction

Berta Maria Martins, Tatiana Svetlitchnaia, and Holger Dobbek*
Laboratorium Proteinkristallographie
Universität Bayreuth
D-95440 Bayreuth
Germany

Summary

2-Oxoquinoline 8-monooxygenase is a Rieske non-heme iron oxygenase that catalyzes the NADH-dependent oxidation of the N-heterocyclic aromatic compound 2-oxoquinoline to 8-hydroxy-2-oxoquinoline in the soil bacterium *Pseudomonas putida* 86. The crystal structure of the oxygenase component of 2-oxoquinoline 8-monooxygenase shows a ring-shaped, C3-symmetric arrangement in which the mononuclear Fe(II) ion active site of one monomer is at a distance of 13 Å from the Rieske-[2Fe-2S] center of a second monomer. Structural analyses of oxidized, reduced, and substrate bound states reveal the molecular bases for a new function of Fe-S clusters. Reduction of the Rieske center modulates the mononuclear Fe through a chain of conformational changes across the subunit interface, resulting in the displacement of Fe and its histidine ligand away from the substrate binding site. This creates an additional coordination site at the mononuclear Fe(II) ion and can open a pathway for dioxygen to bind in the substrate-containing active site.

Introduction

The aerobic soil bacterium *Pseudomonas putida* 86 can use the N-heteroaromatic compound quinoline as a sole source of carbon, nitrogen, and energy. The first step in the bacterial degradation of quinoline is catalyzed by the molybdenum-containing enzyme quinoline 2-oxidoreductase, which hydroxylates the nitrogen-containing ring at the C2 atom, yielding 2-oxo-quinoline, two protons, and two electrons (Bonin et al., 2004). While this first hydroxylation reaction uses water as the source of the incorporated oxygen, the second hydroxylation reaction, catalyzed by 2-oxoquinoline 8-monooxygenase, needs dioxygen, two electrons, and two protons (Figure 1). 2-Oxoquinoline 8-monooxygenase consists of reductase (OMR) and oxygenase (OMO) components that together function to shuttle electrons from the reduced pyridine nucleotide to the active site of OMO, where O_2 activation and 2-oxoquinoline hydroxylation occurs (Rosche et al., 1995b). OMO is a member of a large enzyme family occurring in several aromatic degradation pathways that, as they typically contain a Rieske [2Fe-2S] center next to a mononuclear iron-site, are called Rieske non-heme iron oxygenases (Gibson and Parales, 2000).

*Correspondence: holger.dobbek@uni-bayreuth.de

Oxygenases in general need tight control in O_2 binding and activation to avoid unwanted side reactions. Rieske non-heme iron oxygenases are comprised of two or more proteins, in which both O_2 activation and substrate oxidation take place at the mononuclear non-heme Fe(II) in the oxygenase component (Wolfe et al., 2001, 2002). The two processes are dependent on the binding of substrate at the active site and on the reduction of the Rieske center, implying that the Rieske center affects the affinity of the mononuclear Fe(II) ion for O_2 (Wolfe et al., 2002; Yang et al., 2003a, 2003b). Dependence on substrate or a cofactor to gain O_2 sensitivity at the active site is a common theme in enzymes with a 2-His-1-carboxylate facial triad (Lange and Que, 1998), but regulation by the oxidation state of a second metal site (Rieske center), not directly involved in catalysis, is unique to Rieske non-heme iron oxygenases. Brian Hoffman and coworkers were able to show by deuteron ENDOR measurements that in naphtalene dioxygenase (NDO) reduction of the Rieske center can allosterically modulate the distance between the mononuclear Fe(II) and the substrate (Yang et al., 2003a, 2003b). These observations led to the proposal that Rieske centers can act as regulatory elements in Rieske non-heme iron oxygenases.

To understand the molecular bases of the cooperative effect of Rieske center reduction and O_2 activation in Rieske non-heme iron oxygenases, we determined and compared the crystal structures of OMO in the oxidized, reduced, and substrate bound states. Based on these structures, we demonstrate that the one-electron reduction of the Rieske center results in a restructuring of the hydrogen bonding network across the dimer interface between the Rieske center and the mononuclear Fe(II) ion active site. This rearrangement triggers conformational changes within the active site that can explain the altered affinity of the mononuclear Fe(II) ion for O_2.

Results and Discussion

Overall Structure

The crystal structures of OMO in the oxidized (OMO^{Ox}), reduced (OMO^{Red}), and substrate bound ($OMO^{Ox\text{-}subs}$) states were determined at 1.8 Å resolution (Table 1). The C3-symmetric, ring-like structure of OMO contains six metal centers (Figures 2A and 2B). Each monomer is composed of three domains and coordinates one Rieske center and one mononuclear Fe(II) ion (the active site) (Figures 2C and 2D). The Rieske domain (Figure 2D: residues 40–155, colored in green) is built up by four separate β sheets and binds the Rieske center. The catalytic domain (Figure 2D: residues 16–39 and 156–410, colored in blue) is dominated by a central, seven-stranded, antiparallel β sheet surrounded by loops and α-helical segments and contains the mononuclear Fe(II) ion active site. The small C-terminal trimerization domain (Figure 2D: residues 411–442, colored in orange) consists of one α helix that forms the

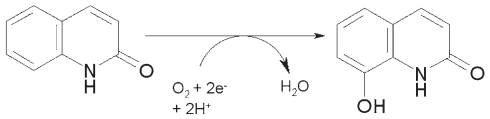

Figure 1. Reaction Catalyzed by 2-Oxoquinoline 8-Monooxygenase

contacts in the center of the trimer (Figure 2A). The dimer contacts are built up by a head-to-tail arrangement of the monomers, positioning the Rieske center of one monomer at a distance of 13 Å from the mononuclear Fe(II) ion active site of another monomer. Upon trimerization, 21.5% of the accessible area of the monomers is buried. While in the buried area, 71.3% has apolar character, the accessible area has 60% apolar character (calculated with the program GetArea 1.1; Fraczkiewicz and Braun, 1998). The trimeric arrangement (α_3) is comparable to that observed for NDO ($(\alpha\beta)_3$) (Kauppi et al., 1998), with an rms deviation of 4.2 Å between the respective monomers (303 of the 427 amino acids of monomeric OMO). Whereas in OMO the trimerization contacts are done by the small C-terminal domain, in NDO, which has no structural equivalent to the C-terminal domain of OMO, the trimerization interface is built up by the β subunit (Figures 2D and 2E).

The active site of OMO is located approximately 8 Å below the protein surface and comprises the mononuclear Fe(II) ion coordinated by the Nϵ atoms of His-221 and His-225, the carboxyl group of Asp-218, and one/two water molecule(s) (Figures 3A and 3B). Mononuclear Fe sites are known to be labile, and their loss leads to the inactivation of the enzyme (Que and Ho, 1996). The mononuclear Fe(II) ion active site of OMO (in all three analyzed states) is fully occupied, as judged by comparing its B factor values with the ones from surrounding atoms.

The Structure of Oxidized OMO

The active site of OMO^{Ox} shows a five-coordinated, distorted tetragonal geometry with one water ligand (Figure 3A). His-221 and His-225 are part of a short, distorted α helix (active site helix, residues 221–225). Asp-218 is positioned directly before this helix, and its carbonyl oxygen is within hydrogen bonding distance to the Nδ atom of His-221 (2.5 Å, Figure 3A). Residual density above the water-ligand of the mononuclear Fe appears to result from a tartrate molecule used for crystallization. The Rieske center is coordinated by two histidines (His-86′ and His-108′; the prime sign refers to the neighboring monomer) and two cysteines (Cys-84′ and Cys-105′) (Figure 3A). The observed average bond lengths between Fe2 - Nδ(His-86′) and Fe2 - Nδ(His-108′) are both 2.23 Å (±0.04 Å). The side chain of His-86′ forms a hydrogen bond across the dimer interface with Asp-361, while the side chain of His-108′ is not involved in hydrogen bonds.

The Structure of Reduced OMO

To avoid possible structural restraints due to crystal packing, OMO^{Red} crystals were obtained by crystallizing previously reduced enzyme. Incubation with 5 mM Na-dithionite under anoxic conditions yields the one-electron reduced Rieske center (as indicated by UV/Vis spectometry and bleaching of the brown color of the obtained crystals). The structure of OMO^{Red} shows a six-coordinated, mononuclear Fe(II) ion site, with two water molecules forming a distorted octahedral geometry (Figure 3B). The observed average bond lengths between Fe2 - Nδ(His-86′) and Fe2 - Nδ(His-108′) for the Rieske center increase to 2.33 Å and 2.36 Å, respectively (±0.04 Å), which corroborates a reduced Rieske center (Cosper et al., 2002). The largest conformational changes are observed at the active site helix (residues 221–225), with shifts between 0.5 and 2.5 Å for the Cα atoms and up to 6 Å for the side chains (Figure 3C). Additionally, there are also new contacts between the two metal sites at the dimer interface. The movement of Asp-218 alters its hydrogen bond network with His-221 (coordinating the mononuclear Fe[II] ion) and with His-108′ (coordinating the Rieske center of the adjacent monomer) (Figure 3C). Whereas in OMO^{Ox} the carbonyl oxygen of Asp-218 is in hydrogen bonding distance with the Nδ of His-221 (Figure 3C: 2.5 Å, colored in blue), in OMO^{Red} the carbonyl oxygen moves away by 1.2 Å, unleashing this interaction. The carboxylate group of Asp-218 swings 2 Å closer to the imidazole side chain of His-221, replacing the former Asp-218 carbonyl to His-221 imidazole hydrogen bond by a side chain to side chain interaction (Figure 3C: 2.8 Å, colored in gray). Thereby, one of the carboxylate oxygens of Asp-218 moves toward His-108′, and the distance of 2.8 Å indicates that a new hydrogen bond across the dimer interface has been formed in OMO^{Red} (Figure 3C: 2.8 Å, colored in gray). Compared to OMO^{Ox}, His-221 is shifted by approximately 1.5 Å in its Cα atom and

Table 1. Phasing Statistics

	Space Group	Unique/ Observed Reflections	R_s[a] Overall/ Last Shell[b]	Resolution (Å)	Completeness (%), Overall/ Last Shell[b]	(I)/ (σI), Overall/ Last Shell[b]	Phasing Power, Centric/ Acentric-Iso/-Ano/	R_{Cullis}[c] Acentric-Iso/Ano	FOM Centric/ Acentric
Native	$C222_1$	49,083/167,903	0.093/0.415	20–2.50	90.8/66.0	10.6/3.0			
PT[d]	$C222_1$	49,267/166,306	0.097/0.447	20–2.50	91.0/70.3	9.8/2.8	1.03/1.19/0.32	0.75/0.98	0.32/0.24

[a] $R_s = \Sigma_h\Sigma_i|I_i(h) - \langle I(h)\rangle|/\Sigma_h\Sigma_i I_i(h)$; where i are the independent observations of reflection h.
[b] Last shell: 2.50–2.60 Å.
[c] $R_{Cullis} = \Sigma_h(||F_{PH}(h) - F_P(h)| - F_{Hcalc}(h))|/\Sigma_h|F_{PH}(h) - F_P(h)|$.
[d] Heavy atom derivative: Pt-$(NH_3)_2(NO_2)_2Cl_2$ with three sites per a.u.

shows a twist of its side chain of 20° (Figure 3C). This movement is transmitted to the mononuclear Fe(II) ion, pushing it approximately 0.8 Å away from the substrate binding pocket (Figure 3C).

Changes Observed upon Reduction

The conformational changes observed at the mononuclear Fe(II) ion upon reduction of the Rieske center (Figure 3C) display the molecular bases needed to understand the regulatory mechanism proposed for Rieske non-heme iron oxygenases (Wolfe et al., 2001, 2002; Yang et al., 2003a, 2003b). We assume that the reduction of OMO by using 5 mM Na-dithionite only influences the redox state of the Rieske center and that the mononuclear Fe(II) ion is already in the ferrous state in the as-isolated enzyme. This is in agreement with the structure of reduced OMO^{Ox} crystals and the reported behavior of other non-heme iron-containing enzymes with a 2-His-1-carboxylate facial triad (Que and Ho, 1996).

The most intriguing structural change in the direct vicinity of the Rieske center is the hydrogen bond between Asp-218 and the Rieske ligand His-108′ that is present in OMO^{Red} but absent in OMO^{Ox} (Figures 3A–3C). This new interaction could arise from two different effects coupled to the reduction of the Rieske center. It could result from the longer bond lengths for Fe2 - Nδ(His-108′) observed in OMO^{Red}, which would move His-108′ toward the subunit interface where Asp-218 is located. However, the increase of the bond length by only 0.1 Å may not be sufficient to explain how such small geometrical changes should hinder the formation of the same hydrogen bond in the oxidized state. An alternative explanation would be to assume a deprotonated state of His-108′ in OMO^{Ox} and its reduction-coupled protonation, corresponding to a change from the oxidized $[(Cys)_2Fe^{III}(\mu_2\text{-}S)_2Fe^{III}(HisH\text{-}86')(His\text{-}108')]^{-1}$ state to the reduced $[(Cys)_2Fe^{III}(\mu_2\text{-}S)_2Fe^{II}(HisH)_2]^{-1}$ state. Changes in the protonation state were suggested to play an important role in the redox cycle of Rieske centers, where the histidine residues can act as acceptors for additional protons, making the reduction potential of Rieske proteins pH dependent (Zu et al., 2001, 2003; Ullmann et al., 2002; Klingen and Ullmann, 2004). Protein-film voltammetry and computational chemistry showed that the interaction of the histidine ligands with the ferric iron in the oxidized state can lower its pK_a value to approximately 7–8, while for the reduced state, the pK_a values are around 5–6 units higher (Zu et al., 2001, 2003; Ullmann et al., 2002). These p*K*a changes have been demonstrated for high-potential Rieske centers, and it's not clear whether it applies equally to low-potential Rieske centers like the one of OMO (Rosche et al., 1995a). However, coupling of reduction of the Rieske center in OMO with the protonation of His-108′ could well explain the newly formed hydrogen bonds. Asp-218 alters its hydrogen bonding network with His-221, thereby causing geometrical changes at the mononuclear Fe(II) ion site. Thus, a reduction-coupled protonation of His-108′ could function as a molecular switch, allowing the cross-communication between the one-electron reduction of the Rieske center and the mononuclear Fe(II) ion active site over a distance of 13 Å. All residues of importance for the proposed mechanism (His-108′, His-221, and Asp-218) are highly conserved within the Rieske non-heme iron oxygenases, and their involvement in the catalytic mechanism has been demonstrated by site-directed mutagenesis. The exchange of Asp-218 for Ala in toluene dioxygenase, anthranilate dioxygenase, and NDO leads to the complete loss of activity (Jiang et al., 1996; Parales et al., 1999; Beharry et al., 2003).

Structural Comparison with NDO

The active site architectures of OMO and NDO are similar in type and arrangement of the ligands (Figures 2D and 2E). However, the conformational changes observed in the different oxidation states of OMO have not been reported for NDO (Kauppi et al., 1998; Carredano et al., 2000; Karlsson et al., 2003). In the NDO structures, the carboxyl group of Asp-205 (Asp-218 in OMO) is hydrogen bonded to His-104′, coordinating the Rieske center (His-108′ in OMO), and to the His-208 ligand of the mononuclear Fe(II) ion (His-221 in OMO). This hydrogen bond network is equivalent to the OMO^{Red} architecture, where the carboxyl group of Asp-218 forms hydrogen bonds with the side chains of His-108′ and His-221 (Figure 3B). X-ray measurements for NDO have been conducted at the synchrotron, and it was shown that the intense X-rays led to the photoreduction of the Rieske center (Karlsson et al., 2000). Thus, the structures reported so far must be seen as that of a reduced state (Kauppi et al., 1998; Carredano et al., 2000; Karlsson et al., 2003). In the present study, OMO crystals were measured by using a rotating-anode X-ray generator that produces less intense X-rays, resulting in considerably decreased photoreduction. The shorter bond lengths for Fe2 histidines of the Rieske center in OMO^{Ox} and $OMO^{Ox\text{-}Subs}$ (discussed below) support the assumption that these structures represent the oxidized state of the enzyme. As the structural differences between OMO^{Ox} and OMO^{Red} likely originate from the protonation/deprotonation of His-108′, the pH during the crystallization process can be another discriminating factor. While crystals of NDO were grown at a pH of 5.8 (Kauppi et al., 1998), crystals of OMO were grown at a pH of 7.5.

The Substrate Bound State

Crystals of OMO^{Ox} soaked with 20 mM 2-oxoquinoline ($OMO^{Ox\text{-}Subs}$) show clear density for a flat aromatic compound in the active site. Omit maps contoured at 5σ define a two-ring system with an additional group sticking out of the ring system, determining the orientation of 2-oxoquinoline (Figure 3D). Refinement of 2-oxoquinoline indicates that the substrate binds directly above the mononuclear Fe(II) ion. The observed average bond lengths between Fe2 - Nδ(His-86′) and Fe2 - Nδ(His-108′) for the Rieske center are comparable to the bond distances in OMO^{Ox} (2.18 Å and 2.19 Å, respectively, with an average error of 0.04 Å). The wall of the substrate binding pocket is mainly built up by hydrophobic and aromatic residues (Figure 3D: Ile-222, Leu-302, Val-304, Trp-307, and Tyr-292), with its end lined up by hydrophilic and charged side chains (Glu-

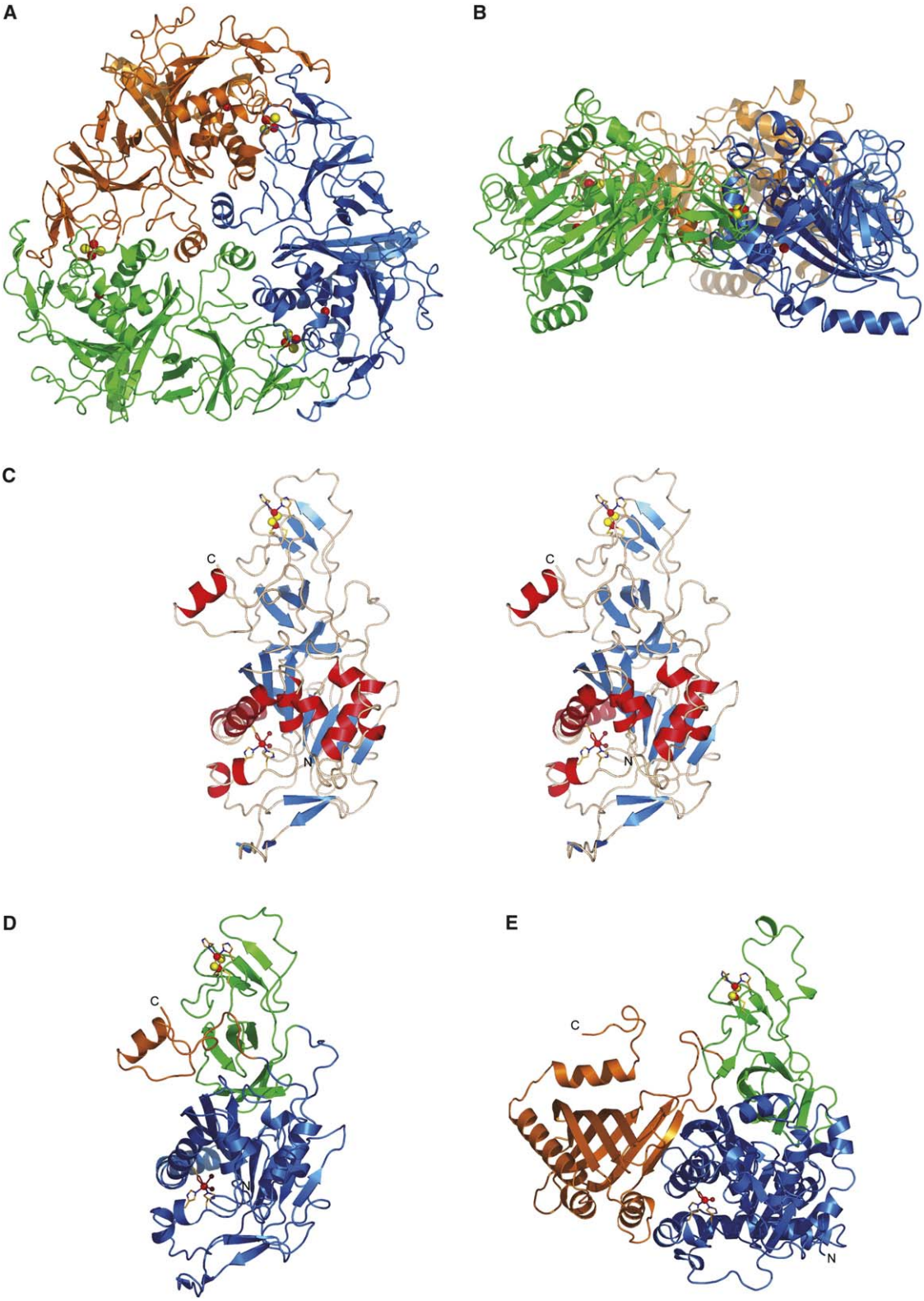

Figure 2. Crystal Structure of OMO

(A and B) Ribbon presentation of the OMO trimer viewed along and perpendicular to the 3-fold symmetry axis, respectively. Monomers are colored differently. The metal sites are shown in ball-and-stick; red, iron; yellow, sulfur.

(C) Stereo representation of the secondary structure topology of the OMO monomer with the N and C termini labeled.

(D) Domain organization of the OMO monomer with the Rieske domain (residues 40–155) shown in green, the catalytic domain (residues 16–

316, Gln-314, and Asn-362). These residues create a flat, elongated compartment in which 2-oxoquinoline is oriented such that its NH group is positioned in hydrogen bonding distance to the carbonyl oxygen of Gly-216 (Figure 3D; 2.7 Å), while its carbonyl group points to the entrance of the pocket. The distance between the mononuclear Fe and the C8 atom of 2-oxoquinoline is 4.7 Å, while the water or hydroxo ligand of the Fe is 2.8 Å apart from the C8 atom (Figure 3D). Upon 2-oxoquinoline binding, small conformational changes occur in the substrate binding pocket, whereas larger movements are found for residues near the entrance of the substrate channel. Residues 235–241 and 273–290 adopt a different conformation in the substrate bound enzyme, with shifts up to 5 Å (Figure 3E). A consequence of this rearrangement is the narrowing of the substrate channel.

Controlling the Access of Dioxygen to the Active Site

The position of 2-oxoquinoline in the active site is determined by (i) a tight fit into the active site pocket, which is obvious from the calculation of van-der-Waals-surfaces, and (ii) a hydrogen bond between its NH group and the carbonyl oxygen of Gly-216. The substrate binding pocket appears to be rigid and positions 2-oxoquinoline close to the mononuclear Fe(II) ion, with its water ligand pointing directly to the bound substrate (Figure 3D).

Binding of 2-oxoquinoline effectively guards the active site against the diffusion of dioxygen to the mononuclear Fe(II) site, as it leaves no pathway for dioxygen. The situation changes when the active site senses the reduction of the Rieske center. The reduction triggers the displacement of both the mononuclear Fe(II) ion and His-221 away from the substrate (around 0.8 Å), which (i) increases the accessible surface at the metal site, and (ii) opens a pathway for dioxygen. Describing the putative steps, one can say that, once protonated, His-108′ attracts Asp-218, which enrolls His-221 in a conformational change that alters the active site geometry and creates a pathway for dioxygen and a new coordination site at the mononuclear Fe(II) ion.

The regulatory role of the oxidation state of the Rieske center is not necessarily restricted to its allosteric function in O_2 binding/activation. During catalysis, the Rieske center becomes reoxidized as it transfers one electron to the mononuclear Fe(II) ion to form the Fe(III)-(hydro)peroxide complex. This most probably results in a coordination geometry similar to the one observed for OMO^{Ox} with restricted coordination space at the metal site. While the open Fe coordination state in OMO^{Red} is well suited to bind O_2 species in a side-on bound state, as observed in NDO (Karlsson et al., 2003), the closed coordination state of OMO^{Ox} would favor end-on bound O_2 species. Thus, our results can explain the regulatory function of Rieske-[2Fe-2S] centers in the catalytic cycle of oxygenases (Yang et al., 2003a, 2003b) and provide a helpful tool for further structural and computational studies on the molecular bases of the reduction-coupled protonation switch mechanism involved in the catalytic cycle of Rieske non-heme iron oxygenases.

Experimental Procedures

Growth Conditions and Protein Purification

P. putida 86 was cultured aerobically in 35 liter fermentors at 30°C in a quinoline minimal medium (Tshisuaka et al., 1993). Whenever quinoline and 2-oxoquinoline were undetectable in the fermentation broth, further portions of quinoline (0.5 ml/l) were added. At an optical density (600 nm) of approximately 3.5, cells were harvested by centrifugation, frozen in liquid nitrogen, and stored at –30°C until further use. The purification protocol included three chromatography steps: ionic exchange with Q-Sepharose fast flow, hydrophobic interaction with Butyl-Sepharose fast flow, and gel permeation with Sephacryl S-200 (all column materials were purchased from Amersham-Pharmacia, Uppsala, Sweden). The pure, homogeneous OMO was concentrated to approximately 50 mg/ml in 10 mM Tris (pH:8.0) was shock frozen in liquid nitrogen, and was stored at –30°C.

Crystallization and Data Collection

Crystallization experiments were carried out by using the hanging drop vapor diffusion method. The optimized aerobic conditions contained a 33%–35% PEG 400, 200 mM ammonium tartrate (pH 6.5) reservoir solution and used a protein to reservoir ratio of 3:2. Mixing of reservoir solution and protein buffer resulted in a pH of 7.5 in the crystallization drop. Crystals appeared after approximately 3 days at 17°C. Crystallizations under anoxic conditions were performed in an anaerobic glove box (Coy Laboratory Products, USA) at a constant temperature of 15°C. The protein was reduced with 5 mM Na-dithionite before crystallization trials. Optimized conditions contained 29%–30% PEG 400, 200 mM ammonium tartrate, 5 mM Na-dithionite (pH 6.5) with a protein to reservoir ratio of 2:2. Crystals appeared within 5 days. Crystals from the same crystallization conditions show space groups $C222_1$ and $P2_12_12_1$ with approximate cell dimensions of 104 × 167 × 173 $Å^3$. Enzyme:substrate complexes were obtained by soaking crystals for 24 hr in crystallization solution containing 20 mM 2-oxo-1,2-dihydroquinoline. Heavy metal derivatization was conducted by soaking crystals for 20 min in crystallization solution containing 1 mM Pt-$(NH_3)_2(NO_2)_2Cl_2$. Crystals were directly frozen in liquid nitrogen, and diffraction data were collected at –180°C on a rotating anode X-ray generator (Nonius FR591, Bruker AXS, Karlsruhe, Germany) equipped with an image plate detector (mar345dtb, marresearch GmbH, Hamburg, Germany).

Structure Solution and Refinement

Isomorphous data were collected at –180°C from a native crystal, and the Pt derivative to a resolution of 2.5 Å. Heavy atom positions were located by difference patterson techniques as implemented in RSPS (CCP4, 1994), and SIRAS phasing was carried out by using SHARP (De La Fortelle et al., 1997) (see Table 1 for details). Phases were modified by solvent flattening by using SOLOMON (CCP4, 1994) and 3-fold cyclic averaging with AVE (Kleywegt and Read, 1997). Model building and refinement were done with MAIN 2000 (Turk, 1992), and positional and temperature refinement were done with CNS (Brünger et al., 1998). The final refinement statistics and stereochemistry analyses performed with PROCHECK (Laskowski

39 and 156–410) shown in blue, and the C-terminal trimerization domain (residues 411–442) shown in orange. Color coding for metal sites is as in (A)–(C).

(E) Subunit organization of the NDO monomer with the Rieske domain (residues 39–159) shown in green and the catalytic domain (residues 1–38 and 160–448) shown in blue (both domains belong to the α subunit), and the β subunit (residues 502–694) shown in orange. Figures 2 and 3 were prepared by using PyMOL (DeLano, 2002).

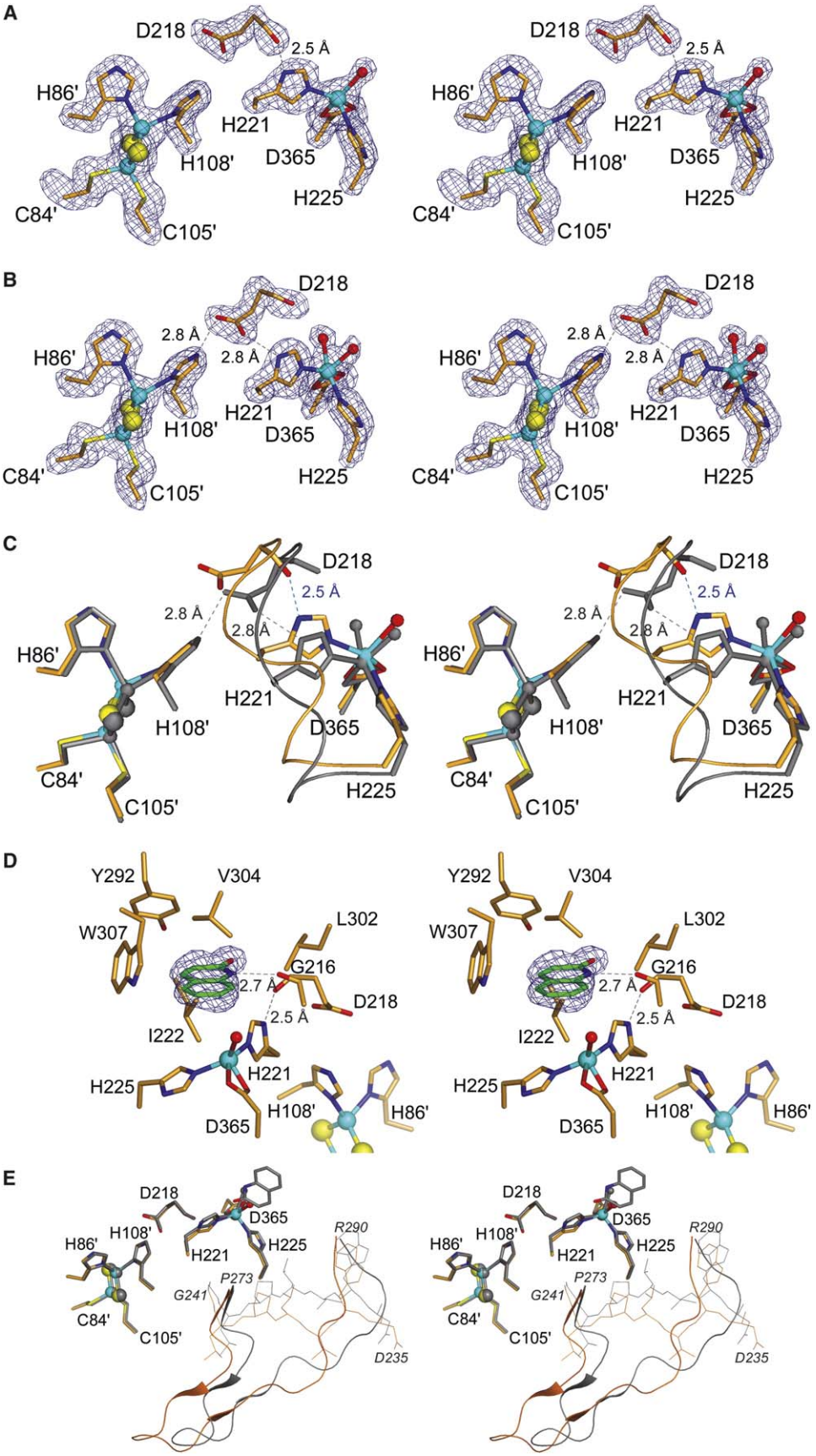
A
D218
2.5 Å
H86'
H221
H108'
D365
H225
C84'
C105'
B
2.8 Å
C
D
Y292
V304
W307
L302
G216
2.7 Å
I222
E
R290
P273
G241
D235

Table 2. Statistics on Diffraction Data and Structure Refinement

Data Set	OMO^{Ox}	OMO^{Red}	$OMO^{Ox\text{-}Subs}$
Total/unique reflections	967,511/275,832	989,855/275,157	968,815/274,366
R_s[a]	0.122 (0.447)	0.123 (0.405)	0.089 (0.478)
Resolution (Å)	20–1.80 (1.9–1.8)	20–1.80 (1.9–1.8)	20–1.80 (1.9–1.8)
Completeness (%)	98.7 (92.0)	99.9 (99.6)	98.2 (93.1)
(I)/(σI)	7.0 (2.6)	8.3 (3.1)	9.7 (2.6)
Model R/R_{free} factor (%)[b]	22.1/26.2	20.6/24.8	20.5/24.3
Rms deviation from ideal geometry			
Bonds (Å)	0.0069	0.0089	0.011
Angles (°)	1.4	1.40	1.36
Ramachandran statistics (%), most favored/additional/generously allowed/disallowed regions	86.0/13.8/0.3/0.0	86.5/13.4/0/0	87.6/12.4/0/0

The Ramachandran statistics are given as defined by PROCHECK (Laskowski et al., 1993). The values given in parantheses are for the highest resolution shell. OMO^{Ox}, OMO crystals grown under oxic conditions; OMO^{Red}, crystals of OMO grown under anoxic conditions in the presence of 5 mM Na-dithionite; $OMO^{Ox\text{-}Subs}$, OMO^{Ox} crystals grown under oxic conditions and soaked with 20 mM 2-oxoquinoline. All three crystals belonged to spacegroup $P2_12_12_1$.

[a] $R_s = \Sigma_h\Sigma_i|I_i(h) - \langle I(h)\rangle|/\Sigma_h\Sigma_i I_i(h)$; where i are the independent observations of reflection h.

[b] The R_{free} factor was calculated from 5% of the data, which were removed at random before the refinement was carried out.

et al., 1993) are shown in Table 2. All distances given in the text are average values of the six independent monomers arranged into two trimers (space group $P2_12_12_1$). Side chain atoms and the "inorganic" part were omitted from the calculation of the difference density ($F_{obs} - F_{calc}$) maps displayed in Figures 3A and 3B.

Acknowledgments

The authors thank S. Fetzner (Universität Münster, Germany) for *P. putida* 86 cultures and helpful discussions, L. Gremer (Universität Bayreuth, Germany) for help in the fermentation, and the departments of biochemistry and crystallography for technical support.

Received: December 30, 2004
Revised: March 1, 2005
Accepted: March 6, 2005
Published: May 10, 2005

References

Beharry, Z.M., Eby, D.M., Coulter, E.D., Viswanathan, R., Neidle, E.L., Phillips, R.S., and Kurtz, D.M., Jr. (2003). Histidine ligand protonation and redox potential in the rieske dioxygenases: role of a conserved aspartate in anthranilate 1,2-dioxygenase. Biochemistry *42*, 13625–13636.

Bonin, I., Martins, B.M., Puranov, V., Fetzner, S., Huber, R., and Dobbek, H. (2004). Active site geometry and substrate recognition of the molybdenum hydroxylase quinoline 2-oxidoreductase. Structure *12*, 1425–1435.

Brünger, A.T., Adams, P.D., Clore, G.M., Delano, W.L., Gros, P., Grosse Kunstleve, R.W., Jiang, J.S., Kuszewski, J., Nilges, M., Pannu, N.S., et al. (1998). Crystallography and NMR system: a new software suite for macromolecular structure determination. Acta Crystallogr. D Biol. Crystallogr. *54*, 905–921.

Carredano, E., Karlsson, A., Kauppi, B., Choudhury, D., Parales, R.E., Parales, J.V., Lee, K., Gibson, D.T., Eklund, H., and Ramaswamy, S. (2000). Substrate binding site of naphthalene 1,2-dioxygenase: functional implications of indole binding. J. Mol. Biol. *296*, 701–712.

CCP4 (Collaborative Computational Project, Number 4) (1994). The CCP4 suite: programs for protein crystallography. Acta Crystallogr. D Biol. Crystallogr. *50*, 760–763.

Cosper, N.J., Eby, D.M., Kounosu, A., Kurosawa, N., Neidle, E.L., Kurtz, D.M., Jr., Iwasaki, T., and Scott, R.A. (2002). Redox-dependent structural changes in archaeal and bacterial Rieske-type [2Fe-2S] clusters. Protein Sci. *11*, 2969–2973.

Figure 3. Crystal Structures of OMO in the Oxidized, Reduced, and Substrate Bound States

(A) Stereo presentation of the active site and the adjacent Rieske center of OMO^{Ox}. Metal center ligands are labeled and shown in sticks; the water ligand is shown as a sphere. Color coding is orange for carbon, blue for nitrogen, red for oxygen, yellow for sulfur, and light blue for iron. The difference density map (F_{obs}-F_{calc}) is shown in blue and is contoured at 5σ.

(B) Stereo presentation of the active site and the adjacent Rieske center of OMO^{Red}. The presentation of atoms and electron density is as in (A).

(C) Stereo presentation of OMO^{Ox} (colored as in [A]) superimposed with OMO^{Red} (in gray). Hydrogen bond interactions are indicated by dashed lines and colored in blue for OMO^{Ox} and in gray for OMO^{Red}. The movement of Asp-218 via its hydrogen bonds with His-221 causes the partial unwinding of the active site helix (residues 221–225).

(D) Stereo presentation of the active site with bound oxoquinoline ($OMO^{Ox\text{-}Subs}$). Representation of atoms is as in (A), except for 2-oxoquinoline (green for carbon). Residues Tyr-292, Val-304, and Trp-307 restrict the access into the substrate binding pocket. Hydrogen bond interactions are indicated by dashed lines. The substrate was omitted for the calculation of the difference density map (F_{obs}-F_{calc}), which is shown in blue and contoured at 5σ.

(E) Ribbon presentation of a superposition of OMO^{Ox} (shown in [A]) and $OMO^{Ox\text{-}Subs}$ (in gray, except for the substrate's carbonyl and nitrogen atoms that are shown in red and blue, respectively). Conformational changes are obvious for residues 235–241 (inner part of the substrate channel; shown as a line for main and side chains with carbonyl atoms omitted for simplicity) and 273–290 (outer part of the substrate channel; shown as a ribbon). The conformational changes depicted result in the lid closure of the substrate channel in $OMO^{Ox\text{-}Subs}$, impeding substrate diffusion from the active site cavity. Thus, the enzyme restricts the access of water to the active site during turnover and minimizes the risk of leakage of not fully processed substrates and/or reaction intermediates.

De La Fortelle, E., Irwin, J.J., and Bricogne, G. (1997). SHARP: a maximum-likelihood heavy-atom parameter refinement and phasing program for the MIR and MAD methods. Crystallographic Computing *7*, 1–9.

DeLano, W.L. (2002). The PyMOL User's Manual (San Carlos, CA: DeLano Scientific).

Fraczkiewicz, R., and Braun, W. (1998). Exact and efficient analytical calculation of the accessible surface areas and their gradients for macromolecules. J. Comp. Chem. *19*, 319–333.

Gibson, D.T., and Parales, R.E. (2000). Aromatic hydrocarbon dioxygenases in environmental biotechnology. Curr. Opin. Biotechnol. *11*, 236–243.

Jiang, H.Y., Parales, R.E., Lynch, N.A., and Gibson, D.T. (1996). Site-directed mutagenesis of conserved amino acids in the alpha subunit of toluene dioxygenase: potential mononuclear non-heme iron coordination sites. J. Bacteriol. *178*, 3133–3139.

Karlsson, A., Parales, J.V., Parales, R.E., Gibson, D.T., Eklund, H., and Ramaswamy, S. (2000). The reduction of the Rieske iron-sulfur cluster in naphthalene dioxygenase by X-rays. J. Inorg. Biochem. *78*, 83–87.

Karlsson, A., Parales, J.V., Parales, R.E., Gibson, D.T., Eklund, H., and Ramaswamy, S. (2003). Crystal structure of naphthalene dioxygenase: side-on binding of dioxygen to iron. Science *299*, 1039–1042.

Kauppi, B., Lee, K., Carredano, E., Parales, R.E., Gibson, D.T., Eklund, H., and Ramaswamy, S. (1998). Structure of an aromatic-ring-hydroxylating dioxygenase-naphthalene 1,2-dioxygenase. Structure *6*, 571–586.

Kleywegt, G.J., and Read, R.J. (1997). Not your average density. Structure *5*, 1557–1569.

Klingen, A.R., and Ullmann, G.M. (2004). Negatively charged residues and hydrogen bonds tune the ligand histidine pK_a values of Rieske iron-sulfur proteins. Biochemistry *43*, 12383–12389.

Lange, S.J., and Que, L., Jr. (1998). Oxygen activating nonheme iron enzymes. Curr. Opin. Chem. Biol. *2*, 159–172.

Laskowski, R.A., MacArthur, M.W., Moss, D.S., and Thornton, J.M. (1993). PROCHECK: a program to check the stereochemical quality of protein structures. J. Appl. Crystallogr. *26*, 283–291.

Parales, R.E., Parales, J.V., and Gibson, D.T. (1999). Aspartate 205 in the catalytic domain of naphthalene dioxygenase is essential for activity. J. Bacteriol. *181*, 1831–1837.

Que, L., Jr., and Ho, R.Y. (1996). Dioxygen activation by enzymes with mononuclear non-heme iron active sites. Chem. Rev. *96*, 2607–2624.

Rosche, B., Fetzner, S., Lingens, F., Nitschke, W., and Riedel, A. (1995a). The 2Fe2S centres of the 2-oxo-1,2-dihydroquinoline 8-monooxygenase from *Pseudomonas putida* 86 studied by EPR spectroscopy. Biochim. Biophys. Acta *1252*, 177–179.

Rosche, B., Tshisuaka, B., Fetzner, S., and Lingens, F. (1995b). 2-Oxo-1,2-dihydroquinoline 8-monooxygenase, a two-component enzyme system from *Pseudomonas putida* 86. J. Biol. Chem. *270*, 17836–17842.

Tshisuaka, B., Kappl, R., Huttermann, J., and Lingens, F. (1993). Quinoline oxidoreductase from *Pseudomonas putida* 86: an improved purification procedure and electron paramagnetic resonance spectroscopy. Biochemistry *32*, 12928–12934.

Turk, D. (1992). Weiterentwicklung eines Programms für Molekülgraphik und Elektronendichte-Manipulation und seine Anwendung auf verschiedene Protein-Strukturaufklärungen (Munich, Germany: TU München.).

Ullmann, G.M., Noodleman, L., and Case, D.A. (2002). Density functional calculation of p K(a) values and redox potentials in the bovine Rieske iron-sulfur protein. J. Biol. Inorg. Chem. *7*, 632–639.

Wolfe, M.D., Parales, J.V., Gibson, D.T., and Lipscomb, J.D. (2001). Single turnover chemistry and regulation of O-2 activation by the oxygenase component of naphthalene 1,2-dioxygenase. J. Biol. Chem. *276*, 1945–1953.

Wolfe, M.D., Altier, D.J., Stubna, A., Popescu, C.V., Munck, E., and Lipscomb, J.D. (2002). Benzoate 1,2-dioxygenase from *Pseudomonas putida*: single turnover kinetics and regulation of a two-component Rieske dioxygenase. Biochemistry *41*, 9611–9626.

Yang, T.C., Wolfe, M.D., Neibergall, M.B., Mekmouche, Y., Lipscomb, J.D., and Hoffman, B.M. (2003a). Modulation of substrate binding to naphthalene 1,2-dioxygenase by Rieske cluster reduction/oxidation. J. Am. Chem. Soc. *125*, 2034–2035.

Yang, T.C., Wolfe, M.D., Neibergall, M.B., Mekmouche, Y., Lipscomb, J.D., and Hoffman, B.M. (2003b). Substrate binding to NO-ferro-naphthalene 1,2-dioxygenase studied by high-resolution Q-band pulsed H-2-ENDOR spectroscopy. J. Am. Chem. Soc. *125*, 7056–7066.

Zu, Y., Fee, J.A., and Hirst, J. (2001). Complete thermodynamic characterization of reduction and protonation of the bc(1)-type Rieske [2Fe-2S] center of *Thermus thermophilus*. J. Am. Chem. Soc. *123*, 9906–9907.

Zu, Y., Couture, M.M., Kolling, D.R., Crofts, A.R., Eltis, L.D., Fee, J.A., and Hirst, J. (2003). Reduction potentials of Rieske clusters: importance of the coupling between oxidation state and histidine protonation state. Biochemistry *42*, 12400–12408.

Accession Numbers

Coordinates have been deposited in the PDB under ID codes 1Z01, 1Z02, and 1Z03.